THE JOURNAL OF PHYSICAL CHEMISTRY C

Article

pubs.acs.org/JPCC

Elastic Strain Energy Effects in Faceted Decahedral Nanoparticles

Srikanth Patala,[†] Laurence D. Marks,[†] and Monica Olvera de la Cruz*[,†,‡]

[†]Department of Materials Science and Engineering and [‡]Department of Chemistry, Northwestern University, Evanston, Illinois 60208, United States

ABSTRACT: Decahedral morphology, with re-entrant surface modifications, is one of the common structures observed in nanoparticles. These motifs, although thermodynamically stable only at very small size ranges, have been experimentally observed to grow up to much larger sizes (100 nm to several micrometers). Whereas the surface energy plays an important role, the contributions of the elastic strain energy are nonnegligible at larger sizes and the effect of stress relaxation due to re-entrant surface faceting is poorly understood. In this article, the volumetric strain energy due to the disclination defect is computed using finite element analysis and the relaxation due to the formation of re-entrant surfaces is shown. Contrary to conventional wisdom, the disclination strain energy is shown to be a nontrivial function of the geometry and in general increases with increasing aspect ratio. The computed strain energies also result in approximately 50% increase in the stability regime than the previously reported results obtained using thermodynamical analysis. Finally, finite element analyses are utilized to explain the commonly observed defect configurations and compute the internal rigid body rotations in these particles.

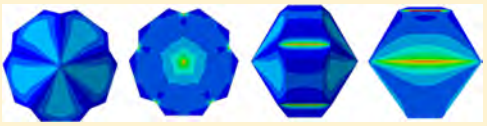

INTRODUCTION

Metallic nanoparticles (NPs) have found applications in a wide variety of technologies. In particular, decahedral-shaped NPs have garnered special attention due to their remarkable plasmonic[1,2] and optical properties[3,4] and due to the possibility of enhanced catalytic activity.[5] There has also been a renewed interest in the decahedral NPs since they exhibit nonconvex polygonal shapes due to re-entrant faceting. Nonconvex shapes offer the possibility of creating new materials through a range of lattice packings with very high densities.[6] Moreover, the pentagonal shapes are inherently strained due to the disclination defect[7] offering distinctive design opportunities such as using the strain energy distribution to alter the local composition of bimetallic nanoparticles to improve their properties. A variety of potential functional applications for decahedral-shaped NPs have led to more practical investigations in their structure, morphology and synthesis.

As important as the chemistry of the decahedral NPs is in governing properties, of equal importance is the structural aspect relating to their morphology. For example, the catalytic properties depend on the crystallographic orientations of the surfaces,[8−10] optical properties are influenced by the size and the shape of NPs,[11−14] and surface functionalization, which is important in many drug delivery applications, depends on the surface structure of NPs.[15,16] Therefore, a precise control of the shapes of NPs during synthesis is of immense technological importance. There have been many experimental advances in nanoparticle syntheses, which allow for the ability to manipulate the size and nanomorphology of decahedral-shaped NPs.[17−22]

Despite the importance of the decahedral NPs and the experimental advances in synthesizing them, there is a lack of rigorous mechanistic understanding of the evolution of their morphology. The contributions of the various key energetic parameters that control the shape of these NPs is unclear. For example, although thermodynamic stability analysis of NPs predict the presence of decahedral shapes only at very small sizes (usually <5 nm),[23,24] these inherently strained structures are observed at much larger sizes and in some cases grow into the micrometer size range.[22,25,26] These large pentatwinned structures are usually grown from solutions and manifest in various geometries with diverse aspect ratios and other features such as re-entrant grooving along the twin boundaries.[27] It has been hypothesized[19,22] that the morphology of the decahedral-shaped nanocrystals can be explained through a combination of kinetic effects and the strain energy contribution. However, such arguments are qualitative and an explicit computation of the shape-dependent volumetric strain energy is missing.

In this article, we use a continuum mechanics approach (with finite element method) to compute the shape-dependent volumetric strain energy in decahedral particles, which is then incorporated in the thermodynamic stability analysis for nanoparticles.[23] Although the role of the volumetric strain energy is not significant in modifying the shape from the thermodynamic shapes computed at small sizes for decahedral NPs,[28] at larger size ranges we show the strain energy contribution due to the disclination defect is significant and the energetically preferred geometry is always the one with a low aspect ratio (pancake-shaped) and high re-entrant grooving.

METHODS

In order to address some of the fundamental questions regarding the growth and stability of these decahedral-shaped NPs and to bridge the gap between experiments and theory, a rigorous thermodynamic stability analysis is essential. One of the most significant energy contributions for decahedral-shaped NPs is the strain energy per unit volume (W_V^D), which depends on the shape of the nanoparticle. The strain in these NPs is generated because unstrained single-crystal segments in the multiply twinned structures

Received: October 10, 2012
Revised: December 21, 2012
Published: January 14, 2013

 © 2013 American Chemical Society dx.doi.org/10.1021/jp310045g | J. Phys. Chem. C 2013, 117, 1485−1494

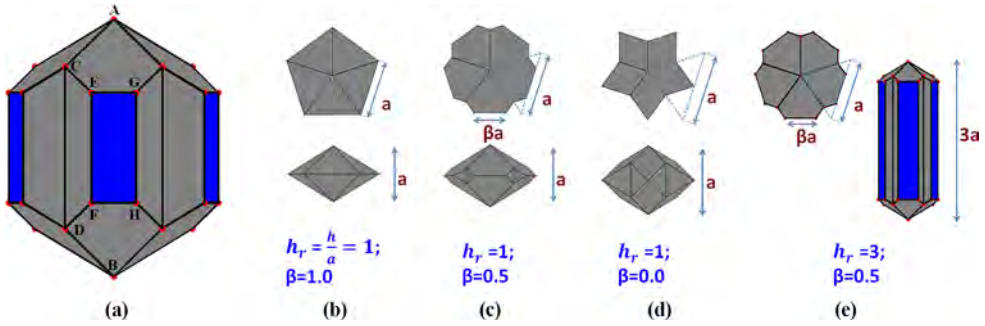

Figure 1. (a) A typical decahedral nanoparticle. The geometric parameters a, β, and h_r are such that $a = AC + CE$, $\beta = (EG/a)$, and $h_r = (AB/a)$. The remaining geometrical units can be expressed as a combination of the parameters a, β, and h_r as $CE = a/2(1-\beta)$, $AC = a/2(1+\beta)$, and $EF = a(h_r - 1)$. β_L is the parameter introduced by Ino and utilized by Marks[28] to describe the grooving factor and is equal to the ratio β/h_r. Parts b, c, d, and e show illustrations of particles with different values of the re-entrant grooving factor β and the aspect ratio h_r.

are not space-filling and the gaps are closed by an angular strain resulting in disclination defects. For example, the decahedral nanoparticles have one disclination line defect along the common line of the five segments and the icosahedral particles have six disclination line defects holding together 20 single crystal segments. In this article, the focus is on the role played by the contribution of the volumetric strain energy of the disclination defect on the stability of the decahedral NPs. We start with an expression of the free energy in terms of the volumetric and surface energy contributions as

$$\begin{aligned} G(T) &= G_V(T) + G_S(T) + (\text{higher order terms}) \\ &\approx V(W_V^D + \Delta\bar{G}_f) + \sum_i A_i(\gamma_i + W_{Si}) + \gamma_t A_t \end{aligned} \quad (1)$$

where V is the volume of the nanoparticle, $\Delta\bar{G}_f$ is the change in free energy per unit volume (from liquid to solid), γ is the surface free energy, W_S is the surface strain energy density term (consisting of the surface stress tensor) and A is the area of the crystallographic facet. The subscript i refers to various crystallographic facets present on the surface and subscript t refers to the {111} twin boundary in the pentatwinned NPs. The higher-order terms comprising the edge and corner energies and the strain energy due to lattice compression (arising from the surface stress) are small except for very small cluster sizes and are neglected here. The advantages of using a multiscale thermodynamic analysis, as compared to atomistic or ab initio simulations, include its applicability to larger size ranges and a wide array of shapes. It is also very powerful since it can applied to different systems (e.g., varying the solution chemistry) by evaluating a minimal number of parameters (surface energies etc.). More recently, such thermodynamic analysis has been successfully used in the Wulff construction of alloy NPs.[29] The applicability of thermodynamic analysis for very small clusters has been validated using atomistic simulations of nickel icosahedral and decahedral structures[24] and will not be discussed further in this article.

The per-volume strain energy W_V^D is expected to vary with geometrical features especially since the re-entrant grooving in these structures can provide elastic stress relaxation.[22,30] Hence it is essential to compute the variation of the elastic strain energy as a function of the geometrical aspects in these structures. Previous studies involving the computation of strain energies have largely been analytical or involved simulations either at the classical ab initio level or at the atomistic level. The analytical studies range from homogeneous isotropic calculations[31,32] to inhomogeneous computations with anisotropic stiffness tensor.[7,23,30,33,34] However, these strain energy computations have been performed only for the distortions in a single-crystal tetrahedral unit without considering more complicated shapes commonly found in practice.

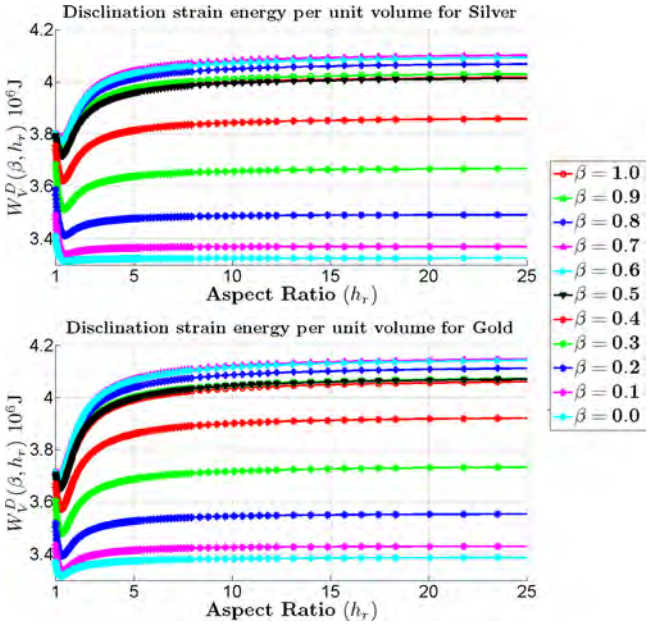

Figure 2. Variation of per-volume strain energy W_V^D with geometric parameters β (grooving factor) in the range [0,1] and h_r (aspect ratio) in the range [1,25].

Classical ab initio methods and atomistic simulations may be used to compute these energies for the complete decahedral nanoparticle; however, these calculations are limited to small sizes and it is difficult to isolate the contribution of the strain energy.[24,35−37] There also exist approximations in these computations—with density functionals in the case of ab initio methods and force-field potentials in the case of atomistic simulations. These methods have also been limited to simple geometries of the decahedral particles.

Finite Element Analysis. In this article, we use a continuum method, the finite element analysis (in ABAQUS[38]), to compute the strain energy density in decahedral-shaped particles with twin boundaries. For completeness we note that for a finite body, with a fixed geometry and without external tractions, the strain energy of the disclination defect is linear with volume if no core cutoff is used. While the stresses and strains for a disclination are nominally singular on the axis, unlike the case for dislocations, the strain energy per unit volume remains finite. Finite element analysis (FEA) is a numerical technique for solving partial differential equations and has been used extensively in a wide variety of engineering problems, especially in the field of elasticity, heat

dx.doi.org/10.1021/jp310045g | J. Phys. Chem. C 2013, 117, 1485−1494

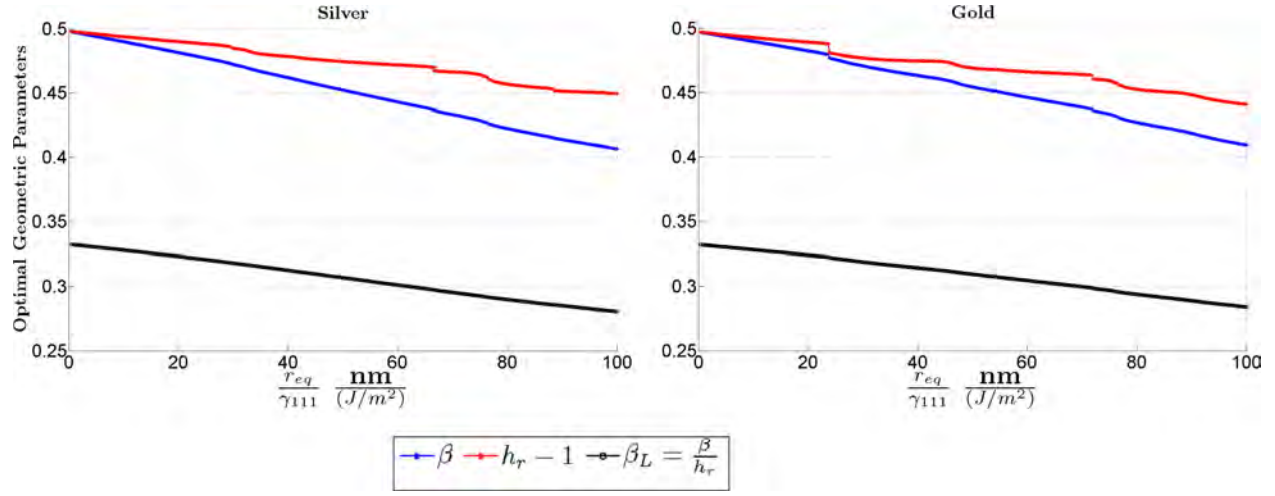

Figure 3. Geometric parameters (β,h_r,β_L) for which the energy in eq 1 is minimized. These plots show a deviation from the modified Wulff form for decahedral nanoparticles,[28] which predicts a constant $\beta_L = (1 - (\gamma_{\{100\}}/(\sqrt{3}\gamma_{\{111\}})))$. These parameters are plotted as a function of the ratio $r_{eq}/\gamma_{\{111\}}$, where $r_{eq} = (3V/4\pi)^{1/3}$, V is the volume of the particle, and $\gamma_{\{111\}}$ is the $\{111\}$ surface free energy.

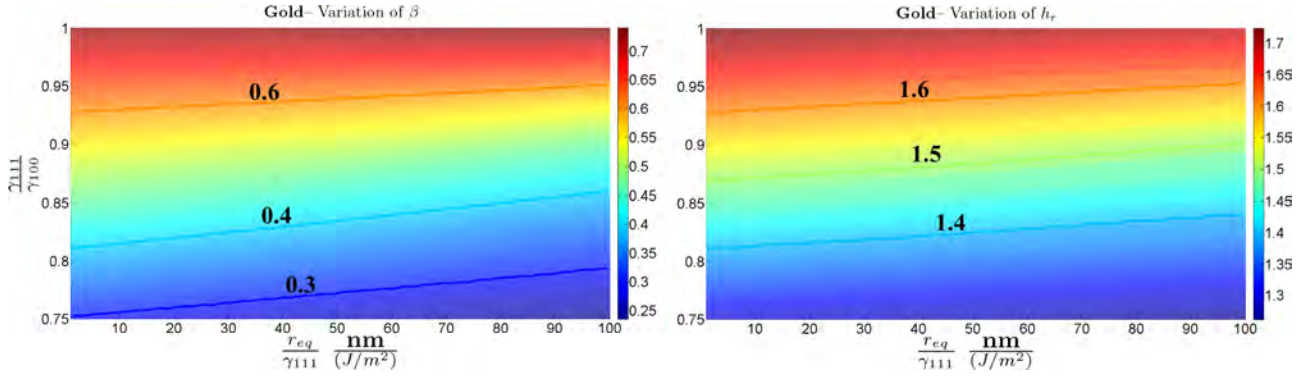

Figure 4. Optimal geometric parameters (a) β and (b) h_r for which the energy in eq 1 is minimized. These parameters are plotted as a function of the ratios $r_{eq}/\gamma_{\{111\}}$ and $\gamma_{\{111\}}/\gamma_{\{100\}}$. Here $r_{eq} = (3V/4\pi)^{1/3}$, V is the volume of the particle, and $\gamma_{\{111\}}$ and $\gamma_{\{100\}}$ are the $\{111\}$ and $\{100\}$ surface free energies, respectively.

Table 1. Comparison of Transition Radii, from Decahedral to Single-Crystal Wulff Shape, Obtained Using the Strain Energy Computed with ABAQUS (Column 2) and HM's[23] Estimate (Column 3) Obtained Using an Isotropic Approximation for the Disclination Strain Energy

material	crossover radius (nm)	Howie–Marks[23] (nm)
gold	~7.78	~5.6
silver	~6.72	~4.7

transfer, and fluid mechanics.[39] The basic idea of FEA is to discretize the space using elements and approximate the solution field through suitable interpolating functions across these elements. This technique allows for solutions of elasticity equations on predefined elements that discretize the complex geometry of the system. This capability makes FEA specially suited for investigating strain energy densities in decahedral NPs with varying aspect ratios and extent of re-entrant grooving. In addition to the flexibility with changing geometry of the particles, FEA facilitates incorporation of nonlinearities, twin boundaries, and elastic anisotropy. The result of this analysis is that the strain energy as a function of the geometric parameters can now be computed, which may be used in the stability analysis for the nonequilibrium decahedral NPs.

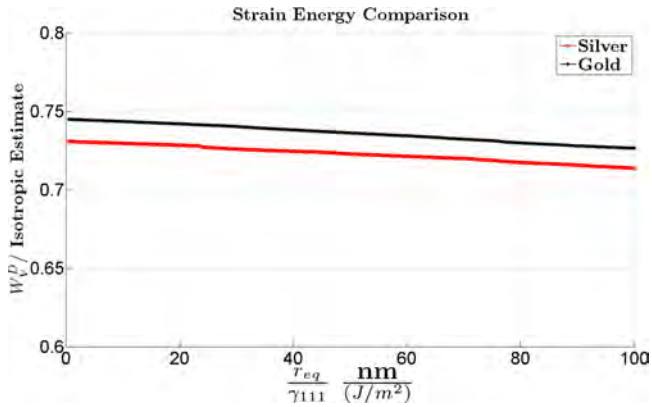

Figure 5. A ratio of the strain energy of decahedral NPs with optimal geometric parameters and the HM estimate of disclination strain energy (isotropic estimate[23]) plotted against $r_{eq}/\gamma_{\{111\}}$. The strain energy obtained using ABAQUS is approximately 75% of the isotropic estimate.

In order to verify the applicability of the FEA for modeling the disclination defect, the strain energies of infinitely long cylinders (simulated using two-dimensional disks with the plane-strain condition[40]) of varying radii with a disclination defect (wedge opening of angle $\Omega^D = 2\pi - 5\arccos(1/3) \sim 7.36°$ to mimic the decahedral NPs) have been computed and compared with de

dx.doi.org/10.1021/jp310045g | J. Phys. Chem. C 2013, 117, 1485–1494

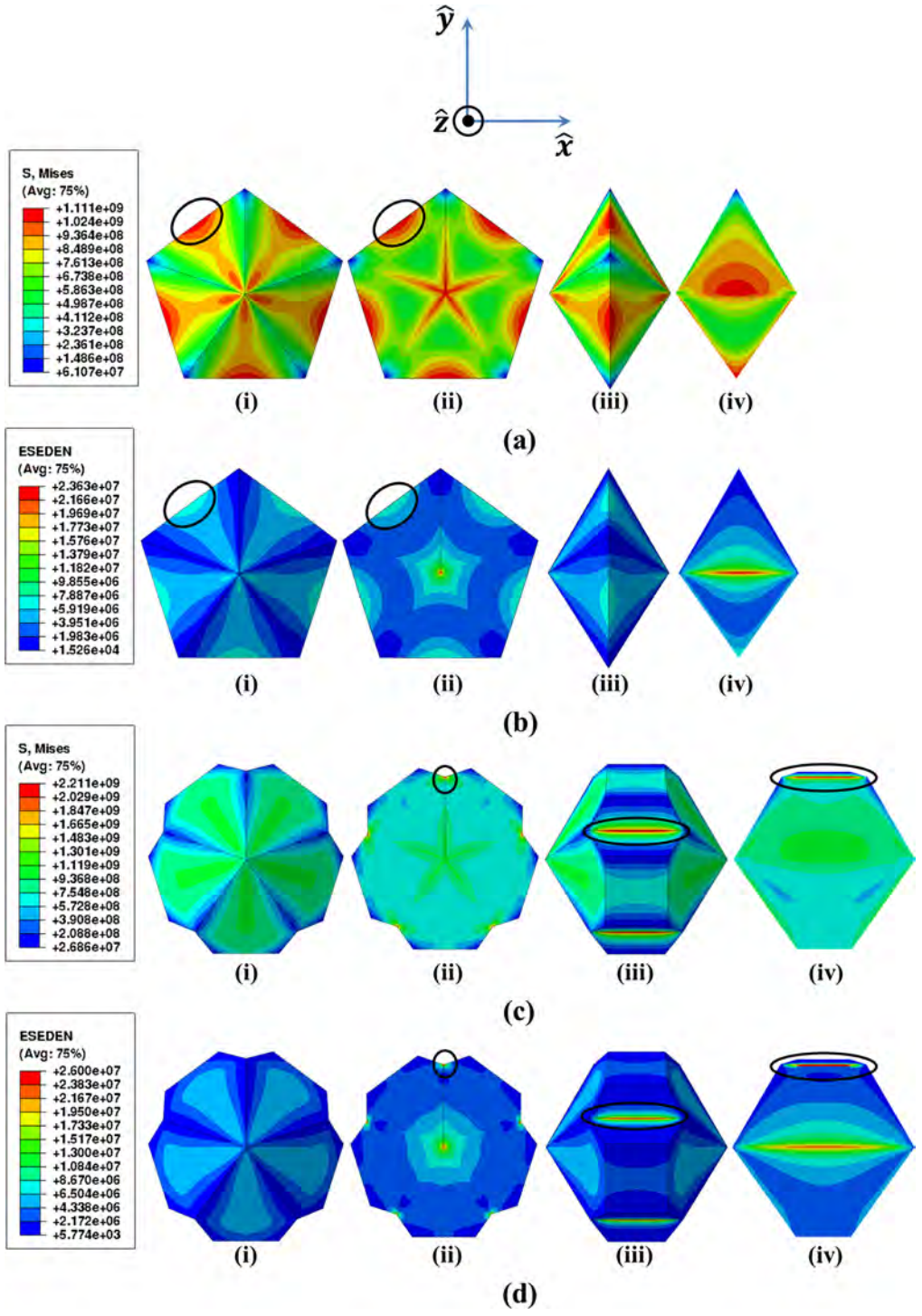

Figure 6. (a,c) Von Mises stress concentration and (b,d) strain energy density profiles in decahedral nanoparticles with geometric parameters: (a,b) $\beta = 1$, $h_r = 1$, and (c,d) $\beta = 0.5$, $h_r = 1.5$. Also shown at the top is the orientation of the Cartesian axes to help understand the views and sections in (i,ii,iii,iv). Suppose this Cartesian system is located at the geometric center of the nanoparticle. The z-axis, which is parallel to the disclination axis in the decahedral shape, is pointing out of the page. The y-axis is in the plane of one of the twin boundaries in the particle. In (i) and (ii), the nanoparticle is viewed along the z-axis direction (i.e., along the disclination axis). The section showed in (ii) represents a cut along the center of the nanoparticle (i.e., along the plane $z = 0$). Shown in (iii) and (iv) is a side view of the nanoparticle along the x-axis and the cut in (iv) is made along the $x = 0$ plane. The stress concentrators and regions of high strain energy density where defects are likely to nucleate are highlighted.

Wit's analytical solution.[7] The details of this analysis and the numerical solutions are provided in Appendix A. An excellent agreement for the strain energies has been obtained validating the applicability of the finite element method for computing the strain energy of the disclination defect in the decahedral nanoparticle systems. We note that the convergence of the finite element analysis to the correct analytical result for a circular two-dimensional disclination is not trivial and hence is an important test.

The analysis of three-dimensional decahedral NPs consists of building a decahedral shape with a wedge gap of angle Ω^D.

dx.doi.org/10.1021/jp310045g | J. Phys. Chem. C 2013, 117, 1485−1494

Boundary conditions are then applied such that the two edges of the wedge match and the wedge is closed. Since the rotational displacement of the edges of the wedge is large, it is necessary to consider the nonlinear terms in the strain tensor. This is termed as the geometric nonlinearity[41] associated with large rotational displacements. The generalized Hooke's law for anisotropic solids[42] is used for the stress−strain relationships in the decahedral NPs. The effect of twin boundaries is modeled by simply dividing the decahedral shaped particle in five equal sections and assigning different crystal orientations to each section such that the misorientation between individual units is compatible with that of a {111} twin boundary. The elastic anisotropy is automatically built in to the system when the different sections (tetrahedral units) are assigned different crystallographic orientations. The analysis is performed in two steps. The first step consists of building the model and applying the boundary conditions such that the wedge gap is closed. In the second step, the boundary conditions closing the wedge are deactivated and a tie constraint (see ABAQUS[38] Analysis User's Manual, Section 31 "Constraints", subsection 3.1 "Mesh tie constraint'" for further details) is applied to the two edges of the wedge to simulate bonding in the system. During this step the system is equilibrated with the tie constraint.

RESULTS AND DISCUSSION

Per-Volume Disclination Strain Energy $W_V^D(\beta, h_r)$. These two steps have been implemented in ABAQUS for different decahedral-shaped particles and their strain energies computed. There are three geometric parameters that are of interest as shown in Figure 1. The length a of the tetrahedral unit is a measure of the lateral extent of the particle. The aspect ratio h_r is defined as the ratio of the length of the particle along the disclination axis and the length a. The grooving factor β is defined as the ratio of the lengths of the tetrahedral unit after and before grooving such that $\beta = 1$ corresponds to the decahedral shape with no re-entrant grooving (Figure 1b) and $\beta = 0$ represents a star-shaped pentatwinned structure (Figure 1d). Also shown in Figure 1a,e are the different crystallographic orientations of the surfaces exposed in these particles. The only two crystallographic facets that are considered (and usually observed) are the {111} and {100} planes (with the {100} planes present only when the parameters are such that $h_r > 1$ and $\beta \neq 0$). Even though there are three independent parameters, the per-volume strain energy is only a function of aspect ratio h_r and grooving factor β and is denoted as $W_V^D(\beta,h_r)$. Any change in the length a simply scales the dimensions of the particle while the geometry remains unchanged. The strain energy per unit volume, $W_V^D(\beta,h_r)$, has been computed for different values of $\beta \in [0,1]$ and $h_r \in [1,25]$ for gold and silver (the relevant constants are listed in Appendix B) and shown in Figure 2.

The variation of W_V^D with respect to aspect ratio (h_r) for a constant grooving factor (β) is nontrivial. There is a common misconception concerning the strain energy density surrounding a disclination defect. Since the strain energy per unit length of an infinite cylinder with a disclination defect is proportional to the square of the radius of the cylinder,[7] it is assumed that adding new material laterally results in a higher increase in the total strain energy (as the radius is increased) as opposed to adding new material along the disclination axis. However, we are concerned with a constant volume problem. Suppose a cylinder of length l and radius R and assume the strain energy density same as that of the infinite cylinder. This would result in the strain energy of $W^D \propto R^2 l$ due to the disclination defect. The quantity W_V^D is constant if the volume remains constant and redistributing the material laterally (increasing the radius and decreasing the length) or along the disclination axis (increasing the length and decreasing the radius) will not change W_V^D. For decahedral NPs, the geometry is complicated by decahedral caps and re-entrant grooving. The distribution of strain energy density is further modified by the presence of twin boundaries. Therefore, a nontrivial variation of $W_V^D(\beta,h_r)$ is observed especially at low values of h_r. $W_V^D(\beta,h_r)$ initially decreases and then increases to plateau at a certain value (denoted here as

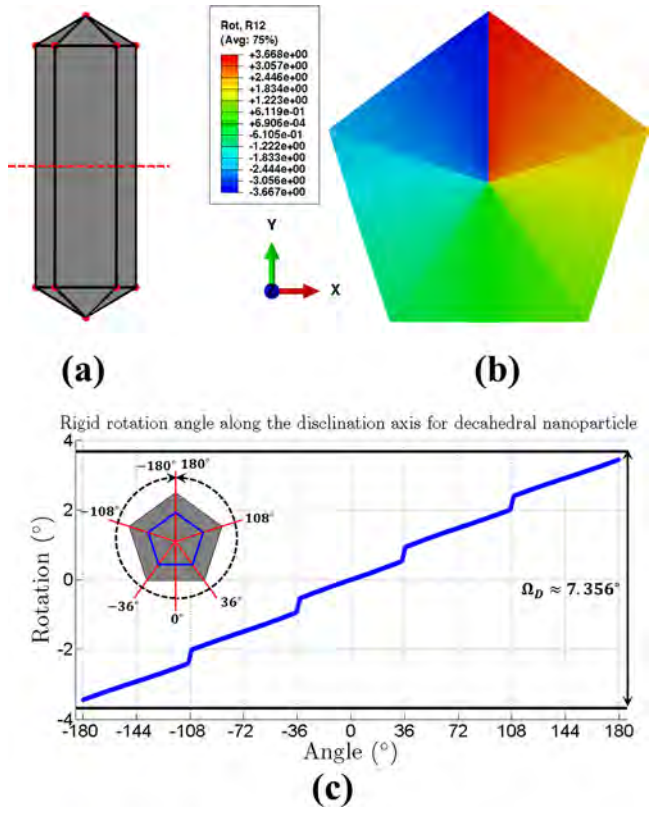

Figure 7. Internal rigid-body rotations along the disclination axis as a function of the angular position. In (a) the geometry of the decahedral rod ($\beta = 1$ and $h_r = 5$) used to compute the rotation tensor along with the plane perpendicular to the disclination axis across which the rotations are plotted is shown. The distribution of the component $\omega_z = (1/2)(\partial u_x/\partial y - \partial u_y/\partial x)$ of the rotation tensor converted to degrees is plotted in (b). In (c), ω_z is plotted along the blue line shown in the inset and the total internal rotation sums up to $\Omega_D \approx 7.36°$.

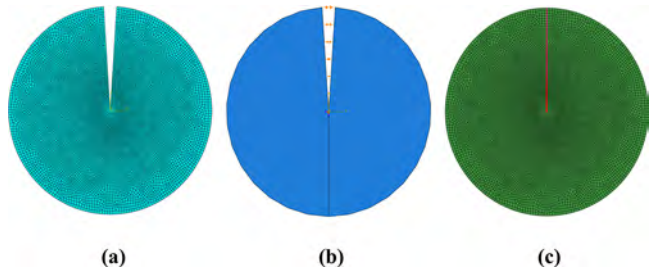

Figure 8. Two-dimensional disk model in finite element analysis software ABAQUS with a wedge disclination angle $\Omega^D \approx 7.36°$ with (a) appropriate meshing and (b) boundary conditions closing the wedge gap. Shown in (c) is the second step in the analysis where the tie constraint is applied to the edges of the wedge and the boundary conditions are removed and the system is equilibrated.

dx.doi.org/10.1021/jp310045g | J. Phys. Chem. C 2013, 117, 1485−1494

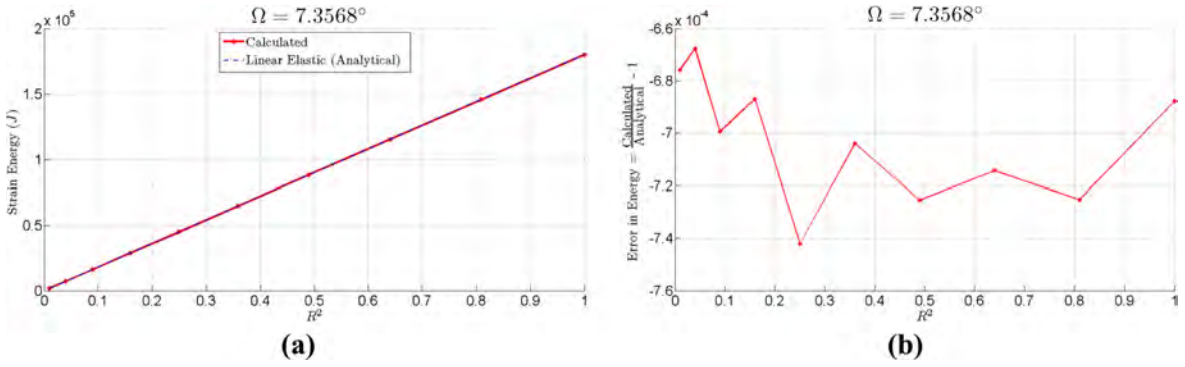

Figure 9. (a) Plots of the analytical deWit solution for the disclination strain energy per unit length for an isotropic infinitely long cylinder and the strain energy computed in ABAQUS for a two-dimensional disk with plane strain condition. Shown in (b) is the error in the energy between the analytical and computed strain energies.

$W_V^D(\beta,\infty)$), which may be greater or lesser than $W_V^D(\beta,0)$ depending on the grooving factor β. The variation of the per-volume strain energy with an increase in re-entrant grooving (a decrease in β) is such that W_V^D initially increases with initial grooving, reaches a maximum around $\beta \approx 0.7$ and then decreases with further increase in grooving. The minimal strain energy is obtained for star-shaped decahedral nanoparticle ($\beta = 0$) with aspect ratio $h_r \approx 1.2$.

Lowest Energy Shapes for decahedral NPs. The thermodynamically most stable decahedral shapes, for any size, may now be obtained by computing the free energy of different shapes using eq 1 and minimizing the energy under the constraint of constant volume. In eq 1, W_V^D is obtained using finite element analysis as described above. The surface free energy parameters ($\gamma_{\{111\}}$ and $\gamma_{\{100\}}$) and the twin boundary energy (γ_t) from Howie−Marks[23] (denoted as HM in the rest of the article) are used in these calculations and are tabulated in Appendix B. As developed by HM, the surface strain energy is assumed to be proportional to the surface energy such that $W_{Si} = g\bar{e}_s\gamma_i$, where $\bar{e}_s = \Omega^D/2$ and g is a constant approximating the surface stress tensor. [The values of g used, to match the computations of HM, are 0.88 and 1 for gold and silver, respectively.] The effect of the strain energy due to lattice compression is negligible[23] compared to the other terms and is not considered for this analysis. The minimization is done numerically and the shape of the faceted decahedral nanoparticle is determined through the optimal geometric parameters β and h_r.

Shown in Figure 3 are the optimal geometric parameters for the decahedral NPs plotted as a function of the ratio $r_{eq}/\gamma_{\{111\}}$. r_{eq}, called the equivalent radius, is a measure of the size of the nanoparticle and is defined as $(3V/4\pi)^{1/3}$, where V is the volume of the nanoparticle. $\gamma_{\{111\}}$ is the surface energy of the {111} crystallographic facet. *The optimal parameters β and h_r vary with the size of the decahedral nanoparticle.* At very low sizes, the contribution of W_V^D is negligible compared to surface terms and the shape is close to the modified Wulff shape formulated by Marks[28] and the geometry is such that $\beta = (1 - (\gamma_{\{100\}}/(\sqrt{3}\gamma_{\{100\}})))h_r$. As the size increases, the contribution of the volume-dependent strain energy starts to dominate and the optimal parameters shift toward the minimum in the $W_V^D(\beta,h_r)$ plot; i.e., the volumetric strain energy drives the system toward star-shaped particles with very low aspect ratios. These results indicate that the growth of elongated decahedral rods is completely a kinetic effect.

It is reasonable to expect the optimal geometric parameters to vary with the surface energies. By systematically varying the surface energies $\gamma_{\{111\}}$ and $\gamma_{\{100\}}$ (e.g., by changing the concentration of surfactants), it is possible to control the shapes of the most stable decahedral nanoparticles. Shown in Figure 4 are the optimal geometric parameters as a function of the ratio of surface energies ($\gamma_{\{111\}}/\gamma_{\{100\}}$) and the parameter ($r_{eq}/\gamma_{\{111\}}$). Although strain energy has an influence on the least energy shapes, as observed in Figures 3 and 4, the effect is weak since the change in shape from the modified Wulff shape (especially in the size range $\lesssim$10 nm) is small.

Table 2. Elastic Constants and the Surface Energy Parameters Used for the Thermodynamic Analysis of the Decahedral-Shaped Nanoparticles of Gold and Silver[a]

material	elastic const (GPa)	$\gamma_{\{111\}}(J/m^2)$	$\gamma_t(J/m^2)$
gold	C_{11} = 192.9; C_{12} = 163.8; C_{44} = 41.5	2.26	0.0175
silver	C_{11} = 124; C_{12} = 93.4; C_{44} = 46.1	1.9	0.01

[a]The elastic constants are from ref 42 and the surface energy parameters are obtained from HM[23] with $\gamma_{\{100\}} = 2\gamma_{\{111\}}/\sqrt{3}$.

Transition Radii. The computed strain energies also have implications for the transition radii from the pentatwinned structure to the single-crystal Wulff shape. Since the model for surface energies and surface strain energy is adopted from HM, a comparison to the transition radii predicted for gold and silver is made in Table 1 with the transition radii obtained in HM. In HM, the elastic strain energy due to the disclination defect is evaluated using isotropic elastic constants. The strain energy of the thermodynamic shape computed using ABAQUS varies with size and is about 75% of the HM's prediction (as shown in Figure 5). The new estimate for the strain energy resulted in ~50% increase in the transitions size radius (see Table 1). This increase in the transition size, although in the right direction, is a large effect. However, this increase is predictable since the strain energy computed in HM using variational methods is an upperbound and is necessarily an overestimate.

Insights from Finite Element Analysis. As the size of the decahedral NPs increases, it is more likely to find crystal lattice defects such as dislocations, stacking faults, etc., in these particles. These lattice defects result in the relaxation of the bulk strain energy (due to the disclination defect) and extend the stability regime of the decahedral motifs. In fact, the re-entrant grooving along the twin boundaries has been proposed to be a mechanism for stress relaxation.[22,30,43] The plots of the per-volume strain energy W_V^D shown in Figure 2 provide evidence for this mechanism. Results from the FE analysis also comprise stress and strain energy density (SED) as a function of position in the decahedral

dx.doi.org/10.1021/jp310045g | J. Phys. Chem. C 2013, 117, 1485−1494

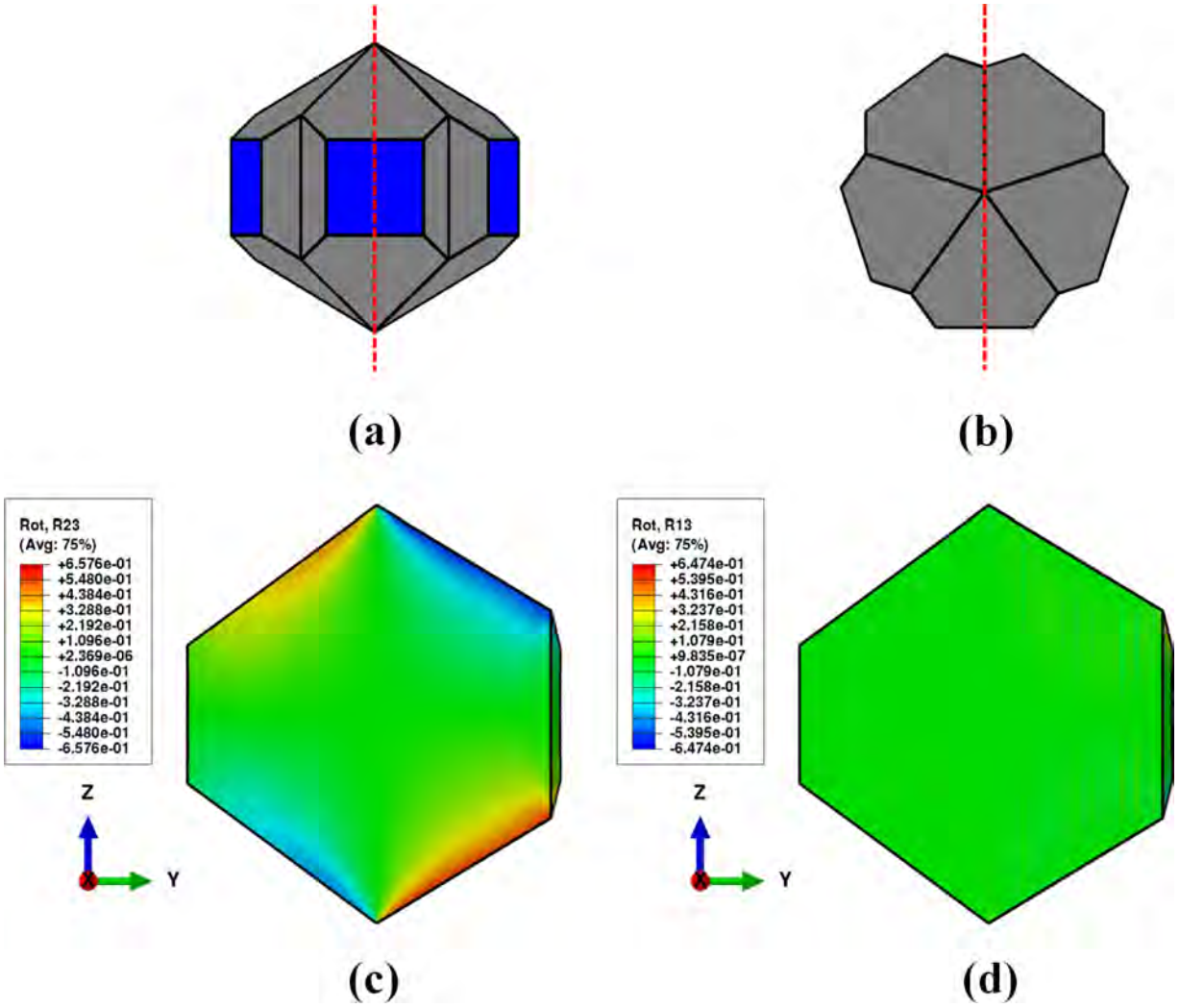

Figure 10. Geometry of the decahedral particle, shown in two different views in (a) and (b). The geometrical parameters are $\beta = 0.5$ and $h_r = 1.5$, which is the modified-Wulff shape when $\gamma_{111}/\gamma_{100} = \sqrt{3}/2$. The red dashed lines represent the plane section, in the decahedral particle, that is perpendicular to the global x-axis and along which the distributions of the rotation tensor components ω_x and ω_y are plotted in (c) and (d), respectively. The magnitudes (in degrees) of the rotation components are very small and the extreme values are only observed close to the surface of the decahedral caps, implying negligible bending in the particle.

nanoparticles. These profiles are utilized to identify regions of high stress (and SED) concentration and to correlate with experimentally observed defect configurations in decahedral NPs. Commonly observed defects in small decahedral NPs are the "wedge-shaped" defect consisting of twinned layers within the individual tetrahedral units and dislocations localized near twin boundaries.[30]

Shown in Figure 6 are the Von Mises stress[44] and SED profiles in two different decahedral-shaped particles. The presence of high stress and SED concentration in the tetrahedral unit (at the center of the outer edge) for $\beta = 1$ NPs (Figure 6a,b) provides the necessary driving force for the nucleation of twinned layers, which are commonly observed in these structures. Similarly, high stress concentrations are found close to the twin boundaries for $\beta \geq 0.5$ (Figure 6c,d) shapes, resulting in stacking fault formation close to the twin boundaries in decahedral NPs with re-entrant grooving.

Another important quantity with relevance to high-resolution electron microscopy (HREM) is the internal rigid-body rotation of the decahedral nanoparticle. The rigid-body rotation has been computed by analyzing the high-resolution electron microscopy (HREM) image with geometric phase analysis.[45] In Figure 7, the internal rotation (equal to the component $\omega_z = (1/2)(\partial u_x/\partial y - \partial u_y/\partial x)$ of the rotation tensor $\omega = (1/2)(\nabla\vec{u} - (\nabla\vec{u})^T)$) is plotted in degrees as a function of angular position in the decahedral particle. As observed in Johnson et al.,[45] the internal rigid-body rotation exhibits discontinuities (of magnitude ~0.25°) across the twin boundaries. However, contrary to the observation in Johnson et al., the internal rotation sums up to $\Omega_D \approx 7.36°$, (the solid angle deficit in the disclination model of the decahedral nanoparticle). We note that a smaller number implies some defect relaxation mechanism. The presence of discontinuities in the internal rotation at the twin boundaries, which may be attributed to the anisotropic nature of the elastic constants, requires further analysis. Also relevant for HREM is the bending of the decahedral particles parallel to the disclination axis. The bending in these particles is investigated using the components ω_x and ω_y of the rotation tensor along the plane sections parallel to the disclination axis. These components are calculated and presented in Appendix C. We observe that these rotation components are negligible in the particle except at the surface of the decahedral caps implying negligible bending of the particle due to the disclination defect.

dx.doi.org/10.1021/jp310045g | J. Phys. Chem. C 2013, 117, 1485−1494

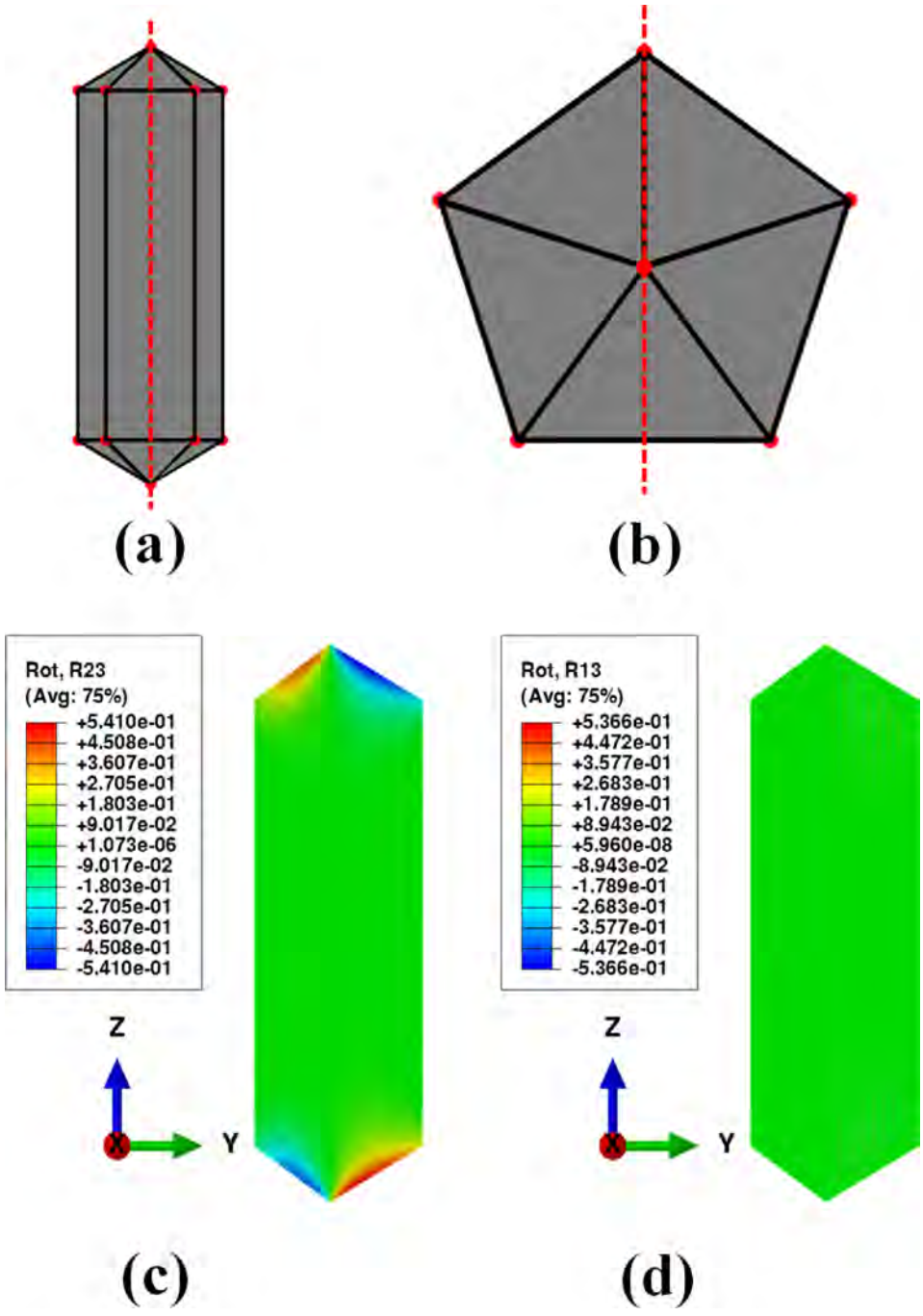

Figure 11. Geometry of the decahedral rod, shown in two different views in (a) and (b). The geometrical parameters are $\beta = 1$ and $h_r = 5$. The red dashed lines represent the plane section, in the decahedral particle, that is perpendicular to the global x-axis and along which the distributions of the rotation tensor components ω_x and ω_y are plotted in (c) and (d), respectively. The magnitudes (in degrees) of the rotation components are very small and the extreme values are only observed close to the surface of the decahedral caps, implying negligible bending in the particle.

CONCLUSIONS

Metallic nanoparticles (NPs) and their assemblies have been utilized in a variety of applications, such as in catalysis, plasmonics, nanoelectronics, biomolecular analysis, and sensing. Since there is a strong correlation between size, shape (morphology), and structure (heterogeneities, defects, etc.) of NPs and their properties, the emphasis during synthesis is on the precise control of these structural aspects. In particular, decahedral NPs offer unique possibilities due to their nonconvex shapes and the presence of inherent strain that could be exploited to control shape and structure.

Although numerous approaches for the synthesis of metallic NPs with a precise control over shape and morphology exist, there is a lack of a complete theoretical basis to help understand the stability and growth kinetics of the decahedral nanostructures. The first step in this direction is to obtain accurate estimates of all the energetic contributions, and in the case of decahedral NPs the strain energy due to the disclination defect is an essential aspect in the thermodynamic equations governing their stability. In order to model the strain energy accurately, the effects of elastic anisotropy, twin boundaries, and the shape of the particle need to be considered. Finite element analysis (FEA) is especially suitable to perform these

dx.doi.org/10.1021/jp310045g | J. Phys. Chem. C 2013, 117, 1485−1494

computations because of the ease with which the anisotropy and nonlinearities can be incorporated and the capability of investigating different geometries. FEA is implemented in ABAQUS to compute the strain energy of decahedral shapes for different geometries by varying two parameters: grooving factor (β) and aspect ratio (h_r).

The variation of per-volume strain energy due to the disclination defect (W_V^D) as a function of the geometric parameters β and h_r is shown to be nontrivial (Figure 2). For a constant β, $W_V^D(\beta,h_r \geq 10)$ can be greater or lesser than $W_V^D(\beta,0)$. Contrary to conventional wisdom suggesting relief of elastic strain energy due to axial growth (i.e., growth along the disclination axis resulting in long decahedral rods), for $\beta = 1$ the strain energy for long rods is larger than those with very low aspect ratio. This result suggests that the growth of long decahedral rods from solutions should be completely a kinetic effect resulting in nonequilibrium shapes. The effect of re-entrant grooving is such that a decrease in strain energy is obtained only after substantial grooving ($\beta \leq 0.5$).

The most stable shapes for the decahedral nanoparticles depend on their size. At very low sizes, the role played by volumetric strain energy is insignificant and the geometry is given by the modified-Wulff shape ($\beta = (1 - (\gamma_{\{100\}}/(\sqrt{3}\gamma_{\{111\}})))h_r$). As the size increases, the contribution of the strain energy starts to dominate and the shape is driven toward the global minima in the $W_V^D(\beta,h_r)$ plot ($\beta = 1$, $h_r \sim 1.2$). To compare the effect of the newly obtained strain energy on the stability regime of the decahedral NPs, a comparison to the estimates obtained in HM is made. About 25% decrease in strain energy as compared to HM's solution results in about a 50% increase in the stability regime. FEA also provides with the stress and strain tensors and the elastic energy density at any location in the decahedral shape. These results show that the distributions of stress and strain energy density are not homogeneous and the regions of high stress concentrations are highlighted in Figure 6. Structural defects such as stacking faults and dislocations have been observed to have nucleated in these regions to relieve elastic strain energy.

APPENDIX A

Finite Element Analysis of the Disclination Defect in a Two-Dimensional Disk

The finite element method is used to first evaluate strain energies per unit length of a disclination defect in an infinitely long cylinder (simulated using a two-dimensional disk with the plane-strain condition) and compared with the strain energy per unit length evaluated analytically[7] (shown in eq 2) for an infinitely long isotropic cylinder.

$$E = \frac{G\Omega^2 R^2}{16\pi(1-\nu)} \tag{2}$$

Here Ω is the angle of the disclination defect, ν is the Poisson's ratio, and G is the shear modulus. The elastic energy is computed using finite element simulation in ABAQUS. A two-dimensional disk model was first built with a wedge gap of angle $2\pi - 5\arccos(1/3)$ (the angle of a disclination defect in a pentatwinned nanoparticle) as shown in Figure 8a. There are two steps involved in the simulation (as mentioned in the section Finite Element Analysis). In the first step, the wedge gap is closed by applying boundary conditions (Figure 8b) on the edges of the wedge such that the edges overlap. In the second step, a tie constraint is applied (to simulate bonding as shown in Figure 8c), the boundary conditions are removed, and the system is equilibrated. Since the strain energy varies as radius squared, strain energies for two-dimensional disks of varying radius have been computed and plotted again the analytical solution in Figure 9a. The calculated and analytical solutions agree well as can be observed from the plot of relative energy differences in Figure 9b.

APPENDIX B

Parameters

The relevant constants and surface energy parameters used for the thermodynamic analysis are listed in Table 2.

APPENDIX C

Column Bending in Decahedral Nanoparticles

An important issue in high-resolution electron microscopy (HREM) of decahedral nanoparticles is concerned with the bending of atomic columns parallel to the decahedral axis. We present here some preliminary results concerning bending that may arise due to the presence of disclination defect using finite element analysis. It is important to note here that we do not consider the effect of surface stresses, which may be important at the size ranges relevant to HREM characterization.

To obtain a complete picture of rotations in decahedral-shaped particles, the infinitesimal rotation tensor $\boldsymbol{\omega}$ is computed. $\boldsymbol{\omega}$ is expressed in terms of gradients of the displacement vector ($\vec{u}$) as

$$\boldsymbol{\omega} = \frac{1}{2}(\nabla\vec{u} - (\nabla\vec{u})^T) = \begin{pmatrix} 0 & -\omega_z & \omega_y \\ \omega_z & 0 & -\omega_x \\ -\omega_y & \omega_x & 0 \end{pmatrix} \tag{3}$$

The rotation components relevant to bending in the decahedral particles are ω_x and ω_y. These components (in degrees) are plotted in a plane (perpendicular to the x-axis) of the decahedral particles for two different geometries in Figure 10 ($\beta = 0.5$ and $h_r = 1.5$) and Figure 11 ($\beta = 1$ and $h_r = 5$). As can be observed from the magnitudes of ω_x and ω_y, the rotations resulting in the bending of atomic columns are negligible (except at the surfaces of the decahedral caps) and should be difficult to observe experimentally.

AUTHOR INFORMATION

Corresponding Author

*E-mail: m-olvera@northwestern.edu.

Notes

The authors declare no competing financial interest.

ACKNOWLEDGMENTS

We thank the NSF MRSEC for support under award no. DMR-1121262, and NERC, an EFRC funded by the DOE Office of Science, under award no. DE-SC0000989. We also thank Dr. Dhiraj Catoor and the anonymous reviewer for insightful discussions and valuable suggestions to improve the quality of the paper.

REFERENCES

(1) Liu, M.; Guyot-Sionnest, P. *J. Phys. Chem. B* **2005**, *109*, 22192−22200.

(2) Pietrobon, B.; McEachran, M.; Kitaev, V. *ACS Nano* **2008**, *3*, 21−26.

(3) Pastoriza Santos, I.; Sanchez Iglesias, A.; Garcia de Abajo, F.; Liz-Marzan, L. *Adv. Funct. Mater.* **2007**, *17*, 1443−1450.

(4) Pietrobon, B.; Kitaev, V. *Chem. Mater.* **2008**, *20*, 5186−5190.

(5) Walsh, M.; Yoshida, K.; Kuwabara, A.; Pay, M.; Gai, P.; Boyes, E. *Nano Lett.* **2012**, *12*, 2027−2031.

(6) de Graaf, J.; van Roij, R.; Dijkstra, M. *Phys. Rev. Lett.* **2011**, *107*, 155501.
(7) DeWit, R. *J. Phys. C: Solid State Phys.* **1972**, *5*, 529.
(8) Gates, B. *Chem. Rev.* **1995**, *95*, 511−522.
(9) Narayanan, R.; El-Sayed, M. *Nano Lett.* **2004**, *4*, 1343−1348.
(10) Cuenya, B. *Thin Solid Films* **2010**, *518*, 3127−3150.
(11) Kelly, K.; Coronado, E.; Zhao, L.; Schatz, G. *J. Phys. Chem. B* **2003**, *107*, 668−677.
(12) Scher, E.; Manna, L.; Alivisatos, A. *Philos. Trans. R. Soc. London, Ser. A: Math., Phys. Eng. Sci.* **2003**, *361*, 241−257.
(13) Gonzalez, A.; Noguez, C. *J. Comput. Theor. Nanosci.* **2007**, *4*, 231−238.
(14) Noguez, C. *J. Phys. Chem. C* **2007**, *111*, 3806−3819.
(15) Chen, L.; Rajh, T.; Jager, W.; Nedeljkovic, J.; Thurnauer, M. *J. Synchrotron Radiat.* **1999**, *6*, 445−447.
(16) Rajh, T.; Nedeljkovic, J.; Chen, L.; Poluektov, O.; Thurnauer, M. *J. Phys. Chem. B* **1999**, *103*, 3515−3519.
(17) Johnson, C.; Dujardin, E.; Davis, S.; Murphy, C.; Mann, S. *J. Mater. Chem.* **2002**, *12*, 1765−1770.
(18) Sun, Y.; Mayers, B.; Herricks, T.; Xia, Y. *Nano Lett.* **2003**, *3*, 955−960.
(19) Lofton, C.; Sigmund, W. *Adv. Funct. Mater.* **2005**, *15*, 1197−1208.
(20) Chen, Y.; Gu, X.; Nie, C.; Jiang, Z.; Xie, Z.; Lin, C. *Chem. Commun.* **2005**, 4181−4183.
(21) Sanchez-Iglesias, A.; Pastoriza-Santos, I.; Perez-Juste, J.; Rodriguez-Gonzalez, B.; Garcia de Abajo, F.; Liz-Marzan, L. *Adv. Mater.* **2006**, *18*, 2529−2534.
(22) Zhang, W.; Liu, Y.; Cao, R.; Li, Z.; Zhang, Y.; Tang, Y.; Fan, K. *J. Am. Chem. Soc.* **2008**, *130*, 15581−15588.
(23) Howie, A.; Marks, L. *Philos. Mag. A* **1984**, *49*, 95−109.
(24) Cleveland, C.; Landman, U. *J. Chem. Phys.* **1991**, *94*, 7376.
(25) Yacaman, M.; Ascencio, J.; Liu, H.; Gardea-Torresdey, J. *J. Vac. Sci. Technol. B: Microelectron. Nanometer Struct.* **2001**, *19*, 1091.
(26) Elechiguerra, J.; Reyes-Gasga, J.; Yacaman, M. *J. Mater. Chem.* **2006**, *16*, 3906−3919.
(27) Hofmeister, H. *Z. Kristallogr.* **2009**, *224*, 528−538.
(28) Marks, L. *Philos. Mag. A* **1984**, *49*, 81−93.
(29) Ringe, E.; Van Duyne, R.; Marks, L. *Nano Lett.* **2011**, *11*, 3399−3403.
(30) Gryaznov, V.; Heydenreich, J.; Kaprelov, A.; Nepijko, S.; Romanov, A.; Urban, J. *Crystal Res. Technol.* **1999**, *34*, 1091−1119.
(31) Ino, S. *J. Phys. Soc. Jpn.* **1966**, *21*, 346−362.
(32) Ino, S. *J. Phys. Soc. Jpn.* **1969**, *27*, 941−953.
(33) Marks, L. *Surf. Sci.* **1985**, *150*, 302−318.
(34) Dundurs, J.; Marks, L.; Ajayan, P. *Philos. Mag. A* **1988**, *57*, 605−620.
(35) Allpress, J.; Sanders, J. *Aust. J. Phys.* **1970**, *23*, 23.
(36) Cleveland, C.; Landman, U.; Schaaff, T.; Shafigullin, M.; Stephens, P.; Whetten, R. *Phys. Rev. Lett.* **1997**, *79*, 1873−1876.
(37) Halicioglu, T.; Bauschlicher, C., Jr *Rep. Prog. Phys.* **1999**, *51*, 883.
(38) ABAQUS. *ABAQUS/Standard Version 6.10-1*; Dassault Systémes Simulia Corp.: Providence, RI, 2010.
(39) Huebner, K.; Dewhirst, D.; Smith, D.; Byrom, T. *The Finite Element Method for Engineers*; John Wiley & Sons: New York, 2008.
(40) Bower, A. In *Applied Mechanics of Solids*; CRC Press: Boca Raton, FL, 2009; pp 70−71.
(41) Taber, L. In *Nonlinear Theory of Elasticity: Applications in Biomechanics*; World Scientific Pub Co. Inc.: Singapore, 2004; Chapter Analysis of Deformation, pp 67−144.
(42) Bower, A. In *Applied Mechanics of Solids*; CRC Press: Boca Raton, FL, 2009; Chapter Constitutive Models: Relations between Stress and Strain, pp 91−93.
(43) Iijima, S. *Jpn. J. Appl. Phys.* **1987**, *26*, 365−372.
(44) Bower, A. In *Applied Mechanics of Solids*; CRC Press: Boca Raton, FL, 2009; p 48.
(45) Johnson, C.; Snoeck, E.; Ezcurdia, M.; Rodrguez-González, B.; Pastoriza-Santos, I.; Liz-Marzán, L.; Hÿtch, M. *Nat. Mater.* **2007**, *7*, 120−124.